Research Article

Event-triggered load frequency control for multi-area power systems based on Markov model: a global sliding mode control approach

Xinxin Lv[1,2], Yonghui Sun[1] ✉, Shiqi Cao[2], Venkata Dinavahi[2]

[1]College of Energy and Electrical Engineering, Hohai University, Nanjing 210098, People's Republic of China
[2]Department of Electrical and Computer Engineering, University of Alberta, Edmonton, T6G 2V4, Canada
✉ E-mail: sunyonghui168@gmail.com

Abstract: In this study, a new method is put forward for the stability and stabilisation analysis of the event-triggered load frequency control (LFC) with interval time-varying delays, considering the global sliding mode controller. To lighten the network bandwidth and save more limited networked resources, the event-triggered scheme is optimised through quantum genetic algorithm, according to different circumstances. Additionally, global sliding mode control (GSMC) scheme is proposed to provide stronger robustness performance, which against the frequency deviation caused by power unbalance or transmission time delays better. Based on the proposed schemes, multi-area LFC for the power system model is formulated as a Markov jump linear system model, considering transmission time delays and external disturbances. By applying improved Lyapunov stability theory, criteria about the stability and stabilisation conditions for multi-area power system can be deduced in terms of linear matrix inequality. Finally, to validate a more realistic LFC application, the proposed event-triggered GSMC is also deployed on Kundur's two-area test system. Simulation studies are carried out to illustrate the effectiveness and superiority of the developed schemes.

1 Introduction

Load frequency control (LFC) is one of the crucial power system control strategies which can be applied to regulate the frequency fluctuations [1–3]. Minimising the unexpected tie-line power flows and frequency variations between interconnected neighbouring areas, attaining optimal transient behaviour in the presence of prescribed overshoot and keeping robustness under modelling uncertainties and non-linearities are all the objectives of LFC [4]. With the development of renewable energies and battery storages, increasingly more renewable energies and battery storages are being integrated into power systems [5, 6]. It is a challenge for the traditional power grid to accommodate the highly intermittent outputs of renewable energies. Thus, an effective LFC scheme is highly needed for the power system, however, the investigation of LFC in power systems can be treated as the research of objective optimisation and robust control.

Numerous control strategies for the LFC scheme have been proposed by experts which devoted are to developing system stabilisation, such as active disturbance-rejection control [7], PID control [8], model predictive control [9] and other strategies. It is noted that sliding mode control (SMC) is another control strategy to solve the LFC scheme [10, 11]. It is well known for its fast response and robust performance [5]. Hence, it can greatly improve system transient performance and preserve the system robustness [12]. Thus, much research for the SMC application has been investigated in power systems [13, 14]. Meanwhile, some improved SMC approaches have been introduced to LFC, such as improved sliding mode design with adaptive learning strategy [15], passivity-based design of sliding mode [16] and second-order sliding mode [17]. However, the robustness of the traditional SMC only exists in the sliding mode stage. To improve the robustness of SMC, the global sliding mode control (GSMC) has been proposed. It should be noted that GSMC has robust stability during the entire control process better than the traditional SMC [18, 19]. Therefore, the GSMC will be investigated in this paper.

It is worth mentioning that open network is an urgent need for future power systems, with the advantage of low cost and flexibility, which can implement the signal transmission and information communication between different power areas. As the open communication infrastructure is introduced to power systems, the practical communication channels of limited bandwidth and network security have captured the researcher's attention. For the event-triggered scheme, the data packets of sampled signals will not be transmitted over the networks unless the predetermined triggering criteria are satisfied. Hence, the event-triggered scheme has the capability of reducing the number of information transmissions [20]. This can be applied to minimise unnecessary communication resources and maximise network bandwidth utilisation. Inevitably, it brings new challenges in power systems, such as transmission time delays, data losses, as well as out-of-order packets. Thus, the event-triggered scheme for LFC has become an area of focus in power systems. For example, an event-triggered approach for LFC with supplementary adaptive dynamic programming was designed in [21]; event-triggered H_∞ LFC for multi-area power systems under hybrid cyber-attacks was investigated in [22]; event-triggered control for consensus problem in multi-agent systems with quantised relative state measurements and the external disturbance was studied in [23]. Although many research results about the event-triggered scheme with LFC are available, its investigation has not been focused on the design of the suitable event-triggered scheme. Therefore, to optimise the system performance under the event-triggered scheme, the quantum genetic algorithm (QGA) is proposed in this paper, which serves as a motivation.

The QGA combines the theory of quantum computing and the genetic algorithm (GA). GA is a global search algorithm that can be used for large search problems. Additionally, quantum computing is an evolutionary emerging interdisciplinary method that can generally minimise the complexity of the algorithm [24]. The highly parallelisable QGA is able to find the optimal solution most quickly and accurately [25]. The QGA has been applied in various fields, such as economic scheduling [26], target detection technology [27], as well as power systems [24]. Therefore, to optimise the network performance, this QGA will be introduced into this paper.
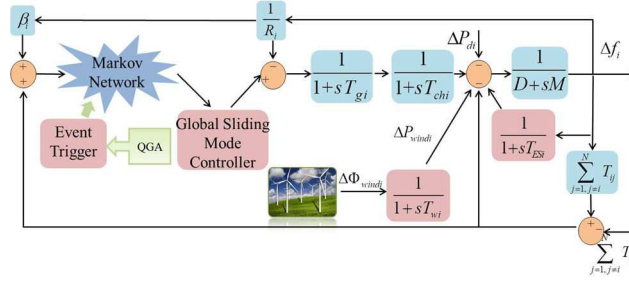
Fig. 1 *Transfer function model of multi-area hybrid power system*

Motivated by the above discussions, this paper investigates the stability and stabilisation of LFC scheme for multi-area power system. Considering the increase in renewable energy sources and energy storage (ES) systems, these aspects are considered in this paper. To reduce the negative influence about transmission time delays and uncertain parameters, the LFC power system with transmission time delays and external disturbances is modelled as a Markov jump linear system. Additionally, GSMC which has better global robustness performance is designed in this paper. To reduce the bandwidth of open network and network utilisation, event-triggered scheme is employed in this paper, and the parameter which determines threshold condition is optimised by QGA. Based on linear matrix inequality (LMI) techniques, the stability and stabilisation criteria are derived under improved Lyapunov function and Wirtinger-based inequality. The main contributions of this work are as follows:

(1) To overcome shortcomings of the conventional SMC with large chattering and slow convergence rate, valid approach GSMC which can ensure global robustness and quick reaching law is designed. However, the power system perturbations, load fluctuations, uncertainty parameters and transmission time delays will reduce the reliability and efficiency of LFC. Therefore, to improve the robustness of LFC for multi-area power system, GSMC is applied in this paper.

(2) To minimise unnecessary communication resources and maximise network bandwidth usage, the event-triggered scheme of LFC for multi-area power system is presented in this paper. In event-triggered scheme, data will not be transmitted to controller unless the threshold condition can be satisfied. In this paper, the parameter of threshold condition is optimised by QGA which combines the theory of quantum computing and GA. Thereby, this event-triggered scheme can be adjusted by different demands.

The remainder of this paper is organised as follows. In Section 2, a Markov jump linear system model for LFC scheme of the multi-area power system is established with event-triggered scheme and GSMC under network conditions. Section 3 shows main results about sufficient stability and stabilisation conditions for LFC of multi-area power systems and robust controller design method with improved Lyapunov function and Wirtinger-based inequality. Moreover, a two-area LFC power system example and a practical test case of Kundur's two-area system which has four synchronous are given in Section 4 to express effectiveness of the method presented in this paper. Finally, the conclusion is presented in Section 5.

2 Dynamic LFC of multi-area power system

The block diagram for the ith control area in multi-area LFC power systems is shown in Fig. 1. Moreover, the signal of area control error (ACE) is assumed to be transmitted to controller over an open network.

The dynamic model of multi-area LFC power systems is shown as follows:

$$\begin{cases} \dot{x}(t) = Ax(t) + Bu(t) + F\omega(t) \\ y(t) = Cx(t) \end{cases} \tag{1}$$

where

$$x_i(t)$$
$$= \begin{bmatrix} \Delta f_i & \Delta P_{mi} & \Delta P_{vi} & \Delta P_{\mathrm{wind}i} & \Delta P_{Bi} & \int ACE_i & \Delta P_{\mathrm{tie}-i} \end{bmatrix}^{\mathrm{T}}$$

$$x(t) = \begin{bmatrix} x_0(t)^{\mathrm{T}} & x_1(t)^{\mathrm{T}} & x_2(t)^{\mathrm{T}} & \ldots & x_n(t)^{\mathrm{T}} \end{bmatrix}^{\mathrm{T}}$$

$$\omega_i(t) = \begin{bmatrix} \Delta P_{di} & \Delta \Phi_{\mathrm{wind}i} \end{bmatrix}^{\mathrm{T}}$$

$$\omega(t) = \begin{bmatrix} \omega_0(t)^{\mathrm{T}} & \omega_1(t)^{\mathrm{T}} & \omega_2(t)^{\mathrm{T}} & \ldots & \omega_n(t)^{\mathrm{T}} \end{bmatrix}^{\mathrm{T}}$$

$$B_i = \begin{bmatrix} 0 & 0 & \left(\dfrac{1}{T_{gi}}\right)^{\mathrm{T}} & 0 & 0 & 0 & 0 \end{bmatrix}^{\mathrm{T}}$$

$$C_i = \begin{bmatrix} \beta_i & 0 & 0 & 0 & 0 & 0 & 1 \\ 0 & 0 & 0 & 0 & 0 & 1 & 0 \end{bmatrix}$$

$$B = \mathrm{diag}\{B_0, \quad B_1, \quad \ldots \quad B_n\}$$

$$C = \mathrm{diag}\{C_0, \quad C_1, \quad \ldots \quad C_n\}$$

$$A_{ii} =$$
$$\begin{bmatrix} (1,1) = \dfrac{-D}{M_i}, (1,2) = \dfrac{1}{M_i}, (1,4) = \dfrac{1}{M_i}, \\ (1,5) = \dfrac{1}{M_i}, (1,7) = \dfrac{-1}{M_i}, (2,2) = \dfrac{-1}{T_{chi}}, \\ (2,3) = \dfrac{1}{T_{chi}}, (3,1) = \dfrac{-1}{RT_{gi}}, (3,3) = \dfrac{-1}{T_{gi}}, \\ (4,4) = \dfrac{-1}{T_{wi}}, (5,1) = \dfrac{1}{T_{ESi}}, (5,5) = -\dfrac{1}{T_{ESi}}, \\ (6,1) = \beta_i, (6,6) = 1, (7,1) = 2\pi \displaystyle\sum_{j=1, j \neq i}^{n} T_{ij} \end{bmatrix}$$

$$A_{ij} = \begin{bmatrix} (7,1) = -2\pi T_{ij} \end{bmatrix}, y_i(t) = \begin{bmatrix} ACE_i & \int ACE_i \end{bmatrix}^{\mathrm{T}}$$

$$F_i = \begin{bmatrix} -\dfrac{1}{M_i} & 0 & 0 & 0 & 0 & 0 & 0 \\ 0 & 0 & 0 & \dfrac{1}{T_{wi}} & 0 & 0 & 0 \end{bmatrix}^{\mathrm{T}}$$

$$A = \begin{bmatrix} A_{11} & \ldots & A_{1n} \\ \vdots & \ddots & \vdots \\ A_{n1} & \ldots & A_{nn} \end{bmatrix}, \quad F = \mathrm{diag}\{F_0, \quad F_1, \quad \ldots \quad F_n\}$$

$$y(t) = \begin{bmatrix} y_0(t)^{\mathrm{T}} & y_1(t)^{\mathrm{T}} & y_2(t)^{\mathrm{T}} & \ldots & y_n(t)^{\mathrm{T}} \end{bmatrix}^{\mathrm{T}}$$

where T_{ij} is the tie-line synchronising coefficient between ith and jth control areas. For the ith control area, $\Delta P_{\mathrm{tie}-i}$ represents tie-line power deviation, ΔP_{di} denotes the load deviation, ΔP_{mi} means the generator mechanical output deviation, ΔP_{vi} indicates the valve

position deviation, $\Delta\Phi_{\text{wind}i}$ is the wind power deviation, $\Delta P_{\text{wind}i}$ is the out of wind turbine generator deviation, ΔP_{Bi} denotes the output power fluctuation of the battery, Δf_i represents the frequency deviation, M_i is the moment of inertia, D_i denotes the generator damping coefficient, T_{gi} means the time constant of the governor, T_{chi} is the time constant of the turbine, R_i means the speed drop, β_i represents the frequency bias factor, $T_{\text{ES}i}$ means the battery time constant, T_{wi} is the wind turbine time constant.

The ACE signal for each control area can be expressed as

$$ACE_i = \beta_i \Delta f_i + \Delta P_{\text{tie}-i} \tag{2}$$

Especially, the GSMC has a fast response and robust performance. Thus, it can improve the system transient performance. Moreover, the integral action is better to enhance anti-interference ability of the system. Therefore, the GSMC will be introduced in this model next.

Thus, the global sliding mode surface function can be constructed as follows:

$$s(t) = \boldsymbol{G}x(t) - \int_0^t \boldsymbol{G}(A - \boldsymbol{BK}C)x(\tau)\mathrm{d}\tau - f(t) \tag{3}$$

where $\boldsymbol{G}$ and $\boldsymbol{K}$ are constant matrices and $\boldsymbol{G}$ is selected to ensure matrix $\boldsymbol{GB}$ to be non-singular.

Remark 1: For GSMC, $f(t)$ is a function that specially designed for achieving global sliding mode, satisfying the following three characteristics :

(1) $f(0) = \boldsymbol{G}x(0)$;
(2) $\lim\limits_{t \to \infty} f(t) = 0$;
(3) the derivative $f(t)$ exists.

Condition (1) signifies that the system state is initially located in the sliding regime. Condition (2) implies the asymptotic stability of the closed-loop system. Condition (3) is required for the existence of a sliding mode. If conditions (1)–(3) are satisfied and the control law is designed such that the sliding condition holds near the sliding regime, asymptotic stability is ensured and the sliding mode exists continually so that robustness is ensured throughout the sliding phase and reaching phase [19]. Hence, $f(t)$ can be designed as follows:

$$f(t) = f(0)e^{-lt} \tag{4}$$

where $l > 0$.

For the ideal global sliding-mode surface, the following function can be satisfied:

$$s(t) = 0, \quad \dot{s}(t) = 0 \tag{5}$$

Thus, the equivalent SMC law is designed as

$$u_{\text{eq}}(t) = -\boldsymbol{K}Cx(t) - (\boldsymbol{GB})^{-1}\boldsymbol{G}F\omega(t) + (\boldsymbol{GB})^{-1}\dot{f}(t) \tag{6}$$

Therefore, the model of power system can be rewritten as

$$\dot{x}(t) = Ax(t) - \boldsymbol{BK}Cx(t) + \tilde{F}\tilde{\omega}(t) \tag{7}$$

where

$$\tilde{F} = [F - B(\boldsymbol{GB})^{-1}\boldsymbol{G}F \quad B(\boldsymbol{GB})^{-1}],$$

$$\tilde{\omega}(t) = [\omega^{\mathrm{T}}(t) \quad \dot{f}^{\mathrm{T}}(t)]^{\mathrm{T}}.$$

For the event-triggered scheme, sampled signals will not be transmitted unless defined triggering criteria can be satisfied [28]. In this way, it can minimise the unnecessary usage of computational and communication resources. Thus, the network

bandwidth utilisation can be maximised. Then, the event-triggered scheme will be presented in this model next. It should be noted that with zero-order hold, the event-triggered scheme can be transferred as follows:

$$[x(t_kh + jh) - x(t_kh)]^{\mathrm{T}}\boldsymbol{\Phi}[x(t_kh + jh) - x(t_kh)] \\ > \lambda x(t_kh)^{\mathrm{T}}\boldsymbol{\Phi}x(t_kh) \tag{8}$$

where $\boldsymbol{\Phi} = [\Phi_0, \quad \Phi_1, \quad \dots \quad \Phi_r]$ is an unknown positive matrix which needs to be designed and $\lambda = [\lambda_0, \quad \lambda_1, \quad \dots \quad \lambda_r] \in [0, 1)$. It means that, if (8) can be satisfied, the sampled data $x(t_kh)$ will be transmitted.

The release times satisfy the next condition

$$t_{k+1}h = \min_j \{t_kh + jh \big| [x(t_kh + jh) - x(t_kh)]^{\mathrm{T}} \\ \boldsymbol{\Phi}[x(t_kh + jh) - x(t_kh)] \\ > \lambda x(t_kh)^{\mathrm{T}}\boldsymbol{\Phi}x(t_kh)\} \tag{9}$$

In the open communication infrastructure, transmission time delay is one of the necessary factors need to be considered. In this way, it needs to consider whether $x(t_kh)$ or $x(t_{k+1}h)$ will be received first. Thus, the two different event-triggered cases are divided by the above condition. If $x(t_kh)$ is received first, define $\tau(t) = t - t_kh$, and $e(k) = 0$. On the contrary, $\tau(t)$ will be defined as

$$\tau(t) = \begin{cases} t - t_kh, & k \in \Omega_0 \\ t - t_kh - mh, & k \in \Omega_m \\ t - t_kh - jh, & k \in \Omega_j \end{cases} \tag{10}$$

where $j = \sup\{m \in N | t_kh + mh < t_{k+1}h, m = 1, 2, \dots\}$, $\tau(t) \in [0, \tau_M]$ and $\tau_M = \max(\tau(t))$, $d = \dot{\tau}(t)$.

At the same time

$$e(t) = \begin{cases} 0, & k \in \Omega_0 \\ x(t_kh) - x(t_kh + mh), & k \in \Omega_m \\ x(t_kh) - x(t_kh + jh), & k \in \Omega_j \end{cases} \tag{11}$$

Under the event-triggered scheme (8), the real transmitted data is

$$u(t) = \boldsymbol{K}y(t_kh) = \boldsymbol{K}Cx(t_kh) \tag{12}$$

By considering transmission time delays, the multi-area power system with event-triggered scheme can be derived as

$$\dot{x}(t) = Ax(t) - \boldsymbol{BK}Ce(t) \\ - \boldsymbol{BK}Cx(t - \tau(t)) + \tilde{F}\tilde{\omega}(t) \tag{13}$$

Remark 2: The open communication network can be modelled as a finite-state Markov process with the following properties:

$$P[r_s(t + \Delta t) = j | r_s(t) = i] = p_{ij}$$

$$0 \le i, j \le L, 0 \le \pi_{ij} \le 1, \sum_{j=0}^{L} \pi_{ij} = 1$$

where π_{ij} is the probability from mode i to mode j, as well as replace the probability of $r_s(t) = i$ to $r_s(t + \Delta t) = j$. It should be noted that Markov jump linear systems can be introduced to study system stability [29], so it is presented in this model.

On the whole, by utilising the Markov jump theory, multi-area LFC power system model based on event-triggered GSMC scheme can be described as the following linear time-invariant system:

$$\dot{x}(t) = Ax(t) - BK_r Ce(t) \\ - BK_r Cx(t - \tau(t)) + \tilde{F}\tilde{\omega}(t) \tag{14}$$

For convenience of analysis, $K(r(t))$ can be denoted as K_r.

Remark 3: To achieve global sliding mode surface, function $f(t)$ is designed in GSMC. By applying the dynamic non-linear sliding mode surface, GSMC eliminates the reaching phase motion of the SMC which will reduce the robust stability of control system. Besides, it has the robustness property all over the control process. Conversely, the robustness of SMC for the parameter uncertainty and external disturbance only exists in sliding mode stage. Therefore, GSMC has better robust performance than traditional SMC [16, 30].

Before presenting the main results, the following lemmas are introduced in advance.

Lemma 1 [31]: Let $\mathbf{Z}_1 = \mathbf{Z}_1^T$, $0 < \mathbf{Z}_2 = \mathbf{Z}_2^T$ and $\mathbf{Z}_3$ be real matrices of appropriate dimensions, then $\mathbf{Z}_1 + \mathbf{Z}_3^T \mathbf{Z}_2^{-1} \mathbf{Z}_3 < 0$, if and only if

$$\begin{bmatrix} \mathbf{Z}_1 & \mathbf{Z}_3^T \\ \mathbf{Z}_3 & -\mathbf{Z}_2 \end{bmatrix} < 0 \quad \text{or} \quad \begin{bmatrix} -\mathbf{Z}_2 & \mathbf{Z}_3 \\ \mathbf{Z}_3^T & \mathbf{Z}_1 \end{bmatrix} < 0.$$

Lemma 2 [32]: For a given matrix $\mathbf{M} > 0$, the following inequality holds for all continuously differentiable function x in $[a, b]$:

$$\int_a^b \dot{x}^T(s)\mathbf{M}\dot{x}(s)\mathrm{d}s \geq \frac{1}{b-a}\zeta_1^T \mathbf{M}\zeta_1 + \frac{3}{b-a}\zeta_2^T \mathbf{M}\zeta_2,$$

where

$$\zeta_1 = x(b) - x(a) \quad \text{and } \zeta_2 = x(b) + x(a) - \frac{2}{b-a}\int_a^b x(s)\mathrm{d}s.$$

Lemma 3 [32]: For given positive integers n, m, a, scalar $\alpha \in (0,1)$, an $n \times n$-matrix $\mathbf{R} > 0$, two $n \times m$-matrices $\mathbf{W}_1$, $\mathbf{W}_2$. Define, for all vector $\boldsymbol{\xi} \in R^m$, the function $\Theta(\alpha, \mathbf{R})$ given by

$$\Theta(\alpha, \mathbf{R}) = \frac{1}{\alpha}\boldsymbol{\xi}^T \mathbf{W}_1^T \mathbf{R}\mathbf{W}_1 \boldsymbol{\xi} + \frac{1}{1-\alpha}\boldsymbol{\xi}^T \mathbf{W}_2^T \mathbf{R}\mathbf{W}_2 \boldsymbol{\xi}.$$

If there is a matrix such that

$$\begin{bmatrix} \mathbf{R} & * \\ X & \mathbf{R} \end{bmatrix} > 0,$$

then the following inequality holds:

$$\min_{\alpha \in (0,1)} \Theta(\alpha, \mathbf{R}) \geq \begin{bmatrix} \mathbf{W}_1\boldsymbol{\xi} \\ \mathbf{W}_2\boldsymbol{\xi} \end{bmatrix}^T \begin{bmatrix} \mathbf{R} & * \\ X & \mathbf{R} \end{bmatrix}\begin{bmatrix} \mathbf{W}_1\boldsymbol{\xi} \\ \mathbf{W}_2\boldsymbol{\xi} \end{bmatrix}$$

3 Stability and performance analysis under QGA

3.1 Stability and stabilisation analysis

In this section, the stability and stabilisation of Markov jump linear system (14) with transmission time delays are analysed based on the event-triggered scheme and GSMC. By utilising optimisation algorithm of QGA, the H_∞ performance index γ under different λ condition is investigated. First, the stability of system (14) with $\tilde{\omega}(t) = 0$ will be presented in the next theorem.

Theorem 1: For given positive constant λ, d, τ_M, the system (14) with $\tilde{\omega}(k) = 0$ is asymptotically stable, if there exist positive definite matrices $\mathbf{P}_r$, $\mathbf{Q}_r$, $\mathbf{R}_r$, $\mathbf{Z}_r$, $\mathbf{S}$, $\mathbf{W}$, $\boldsymbol{\Phi}$ and appropriate dimensions $\mathbf{X}_{1r}$, $\mathbf{X}_{2r}$, $\mathbf{X}_{3r}$, $\mathbf{X}_{4r}$ such the following matrix inequalities hold for all $r = 0, \ldots, L$

$$\begin{bmatrix} \Xi_{1r} & * & * \\ \Xi_{2r} & -\tau_M^{-2}\mathbf{Z}_r & * \\ \Xi_{3r} & 0 & -(\tau_M/2)^{-2}\mathbf{W} \end{bmatrix} < 0$$

$$S'_r = \sum_{j=1}^L \pi_{rj}(\mathbf{Q}_j + \mathbf{R}_j) - \mathbf{S} < 0 \tag{15}$$

$$S''_r = \sum_{j=1}^L \pi_{rj}\mathbf{R}_j - \mathbf{S} < 0, \quad \tilde{\Sigma}_r = \begin{bmatrix} \Sigma_r & * \\ X_r^T & \Sigma_r \end{bmatrix} > 0$$

where

$$\Xi_{1r} = e_1^T \mathrm{E}_{1r}e_1 - e_3^T(1-d)\mathbf{Q}_r e_3 + e_4^T \mathbf{R}_r e_4 + 2e_1^T \mathbf{P}_r \Xi_{4r}$$
$$\quad - \mathrm{E}_{2r}^T \tilde{\Sigma}_r \mathrm{E}_{2r} + \mathrm{E}_{3r}^T \tilde{\phi}_r \mathrm{E}_{3r} - e_2^T \boldsymbol{\Phi} e_2 + \lambda e_3^T \boldsymbol{\Phi} e_3$$

$$\Xi_{2r} = \mathbf{Z}_r Ae_1 - \mathbf{Z}_r BK_r Ce_2 - \mathbf{Z}_r BK_r Ce_3$$
$$\Xi_{3r} = \mathbf{W}Ae_1 - \mathbf{W}BK_r Ce_2 - \mathbf{W}BK_r Ce_3$$
$$\Xi_{4r} = Ae_1 - BK_r Ce_2 - BK_r Ce_3$$

$$\mathrm{E}_{1r} = \sum_{j=1}^L \pi_{rj}\mathbf{P}_j + \mathbf{Q}_r + \mathbf{R}_r + \tau_M \mathbf{S}$$

$$\mathrm{E}_{2r} = \begin{bmatrix} e_1 - e_3 \\ e_1 + e_3 - e_5 \\ e_3 - e_4 \\ e_3 + e_4 - e_7 \end{bmatrix}, \quad X_r = \begin{bmatrix} X_{1r} & X_{2r} \\ X_{3r} & X_{4r} \end{bmatrix}$$

$$\phi_r = \tau_M \sum_{j=1}^L \pi_{rj}\mathbf{Z}_j - \mathbf{W}, \quad \phi_{1r} = \tau_M \sum_{j=1}^L \pi_{rj}\mathbf{Z}_j - \mathbf{S},$$

$$\tilde{\phi}_r = \begin{bmatrix} -\dfrac{2}{\tau_M^2}\phi_r & \dfrac{2}{\tau_M^2}\phi_r \\ \dfrac{2}{\tau_M^2}\phi_r & -\dfrac{2}{\tau_M^2}\phi_r \end{bmatrix}, \quad \Sigma_r = \begin{bmatrix} \dfrac{1}{\tau_M}\phi_{1r} & * \\ 0 & \dfrac{3}{\tau_M}\phi_{1r} \end{bmatrix}$$

$$\mathrm{E}_{3r} = \begin{bmatrix} \tau_M e_1 \\ e_6 \end{bmatrix}, \quad e_j = [\underbrace{0\ldots0}_{j-1}, 1, \underbrace{0\ldots0}_{7-j}], (j = 1, \ldots, 7)$$

Proof: Define the Lyapunov function as (see equation below), where $\mathbf{P}_r$, $\mathbf{Q}_r$, $\mathbf{R}_r$, $\mathbf{Z}_r$, $\mathbf{S}$, $\mathbf{W}$ are positive-definite matrices with appropriate dimensions.□

Calculating the derivative of $V(t)$ along the trajectory (14) with $\tilde{\omega}(k) = 0$, one has

$$\Delta V(t) = \Omega_1 + \Omega_2 + \Omega_3 + \Omega_4 + \Omega_5 \tag{16}$$

where

$$\Omega_1 = x^T(t)\mathrm{E}_{1r}x(t) - x^T(t - \tau(t))(1 - d)\mathbf{Q}_r$$

$$V(t) = x^T(t)\mathbf{P}_r x(t) + \int_{t-\tau(t)}^t x^T(\alpha)\mathbf{Q}_r x(\alpha)\mathrm{d}\alpha$$

$$+ \int_{t-\tau_M}^t x^T(\alpha)\mathbf{R}_r x(\alpha)\mathrm{d}\alpha + \tau_M \int_{-\tau_M}^0 \int_{t+\beta}^t \dot{x}^T(\alpha)\mathbf{Z}_r \dot{x}(\alpha)\mathrm{d}\alpha\mathrm{d}\beta$$

$$+ \int_{-\tau_M}^0 \int_{t+\beta}^t x^T(\alpha)Sx(\alpha)\mathrm{d}\alpha\mathrm{d}\beta + \int_{-\tau_M}^0 \int_\theta^0 \int_{t+\beta}^t \dot{x}^T(\alpha)W\dot{x}(\alpha)\mathrm{d}\alpha\mathrm{d}\beta\mathrm{d}\theta$$

$$x(t - \tau(t)) - x^{\mathrm{T}}(t - \tau_M)\boldsymbol{R}_r x(t - \tau_M) + 2x^{\mathrm{T}}(t)\boldsymbol{P}_r \dot{x}(t)$$
$$+\dot{x}^{\mathrm{T}}(t)\left(\tau_M^2 \boldsymbol{Z}_r + \frac{\tau_M^2}{2}W\right)\dot{x}(t),$$

$$\Omega_2 = \int_{t-\tau(t)}^{t} x^{\mathrm{T}}(\alpha)\left[\sum_{j=1}^{L}\pi_{rj}(Q_j + R_j) - S\right]x(\alpha)\mathrm{d}\alpha,$$

$$\Omega_3 = \int_{t-\tau_M}^{t-\tau(t)} x^{\mathrm{T}}(\alpha)\left[\sum_{j=1}^{L}\pi_{rj}R_j - S\right]x(\alpha)\mathrm{d}\alpha,$$

$$\Omega_4 = -\int_{t-\tau_M}^{t}\dot{x}^{\mathrm{T}}(\alpha)\phi_{1r}\dot{x}(\alpha)\mathrm{d}\alpha, \quad \Omega_5 = \int_{-\tau_M}^{0}\int_{t+\beta}^{t}\dot{x}^{\mathrm{T}}(\alpha)\phi_r\dot{x}(\alpha)\mathrm{d}\alpha.$$

If $S'_r < 0$ and $S''_r < 0$ can be satisfied, next inequality can be obtained with event-triggered scheme

$$\begin{aligned}\Delta V(t) &< \Omega_1 + \Omega_4 + \Omega_5 - e^{\mathrm{T}}(t)\Phi e(t) \\ &+\lambda x^{\mathrm{T}}(t-\tau(t))\Phi x(t-\tau(t))\end{aligned} \quad (17)$$

By applying Lemmas 2 and 3, Ω_4 and Ω_5 can be equivalent to the following inequalities, respectively:

$$\begin{aligned}\Omega_4 &= -\int_{t-\tau(t)}^{t}\dot{x}^{\mathrm{T}}(\alpha)\phi_{1r}\dot{x}(\alpha)\mathrm{d}\alpha - \int_{t-\tau_M}^{t-\tau(t)}\dot{x}^{\mathrm{T}}(\alpha)\phi_{1r}\dot{x}(\alpha)\mathrm{d}\alpha \\ &\leq -\varphi_1^{\mathrm{T}}\Sigma_r\varphi_1 - \varphi_2^{\mathrm{T}}\Sigma_r\varphi_2 \leq \tilde{\varphi}^{\mathrm{T}}\tilde{\Sigma}_r\tilde{\varphi}\end{aligned}$$

$$\begin{aligned}\Omega_5 &= -\frac{\tau_M^2}{2}\int_{-\tau_M}^{0}\int_{t+\beta}^{t}\dot{x}^{\mathrm{T}}(\alpha)\left(-\frac{2}{\tau_M^2}\phi_r\right)\dot{x}(\alpha)\mathrm{d}\alpha \\ &\leq \left[\tau_M x(t) \quad \int_{t-\tau_M}^{t}x(\alpha)\mathrm{d}\alpha\right]\tilde{\phi}_r \\ &\quad \left[\tau_M x(t) \quad \int_{t-\tau_M}^{t}x(\alpha)\mathrm{d}\alpha\right]^{\mathrm{T}}\end{aligned}$$

where $\tilde{\varphi} = \begin{bmatrix}\varphi_1^{\mathrm{T}} & \varphi_2^{\mathrm{T}}\end{bmatrix}^{\mathrm{T}}$

$$\varphi_1 = \begin{bmatrix}x(t) - x(t-\tau(t)) \\ x(t) + x(t-\tau(t)) - \dfrac{2}{\tau(t)}\displaystyle\int_{t-\tau(t)}^{t}x(\alpha)\mathrm{d}\alpha\end{bmatrix}$$

$$\varphi_2 = \begin{bmatrix}x(t-\tau(t)) - x(t-\tau_M) \\ x(t-\tau(t)) + x(t-\tau_M) - \dfrac{2}{\tau_M - \tau(t)}\displaystyle\int_{t-\tau_M}^{t-\tau(t)}x(\alpha)\mathrm{d}\alpha\end{bmatrix}$$

Thus, the following inequality can be yielded:

$$\begin{aligned}\Omega &= \Omega_1 + \Omega_4 + \Omega_5 - e^{\mathrm{T}}(t)\Phi e(t) \\ &+\lambda x^{\mathrm{T}}(t-\tau(t))\Phi x(t-\tau(t)) < 0\end{aligned} \quad (18)$$

Defining the following augmenting state variable:

$$\begin{aligned}\xi_1(t) = \Big[&x(t) \quad e(t) \quad x(t-\tau(t)) \quad x(t-\tau_M) \\ &\frac{2}{\tau(t)}\int_{t-\tau(t)}^{t}x(\alpha)\mathrm{d}\alpha \int_{t-\tau_M}^{t}x(\alpha)\mathrm{d}\alpha\frac{2}{\tau_M - \tau(t)}\int_{t-\tau_M}^{t-\tau(t)}x(\alpha)\mathrm{d}\alpha\Big]^{\mathrm{T}}\end{aligned}$$

Recalling (18), we have

$$\Omega = \xi_1^{\mathrm{T}}(t)\Xi_r\xi_1(t) \quad (19)$$

where

$$\Xi_r = \Xi_{1r} + \Xi_{2r}^{\mathrm{T}}(\tau_M^2 \boldsymbol{Z}_r)^{-1}\Xi_{2r} + \Xi_{3r}^{\mathrm{T}}\left(\frac{\tau_M^2}{2}W\right)^{-1}\Xi_{3r}.$$

Thus, if $\Omega < 0$ can be satisfied, (15) can be verified by applying Lemma 1. Considering a sufficiently small scalar $c \in (0, 1]$, we can

obtain that $\Delta V(k) < \xi_1^{\mathrm{T}}(t)\Xi_r\xi_1(t) < -c\|\xi_1(t)\|^2 < 0$. Therefore, system (14) with $\tilde{\omega}(t) = 0$ is stochastically stable holds for any small scalar $c \in (0, 1]$.

Remark 4: This theorem provides a sufficient and unnecessary condition about the stability of system (14) with $\tilde{\omega}(k) = 0$. In this proof of the theorem, an efficient Lyapunov function is constructed. It includes a triple-integral term $\int_{-\tau_M}^{0}\int_{\theta}^{0}\int_{t+\beta}^{t}\dot{x}^{\mathrm{T}}(\alpha)W\dot{x}(\alpha)\mathrm{d}\alpha\mathrm{d}\beta\mathrm{d}\theta$ and fewer decision variables. In this way, it can acquire less conservative results of multi-area power systems. It should be noted that the inequalities scaling method is applied in Theorem 1. Thus, the conservative problem needs to be considered. In the process of calculation, the Ω_4 is divided into two categories of $\int_{t-\tau(t)}^{t}\dot{x}^{\mathrm{T}}(\alpha)\phi_r\dot{x}(\alpha)\mathrm{d}\alpha$ and $\int_{t-\tau_M}^{t-\tau(t)}\dot{x}^{\mathrm{T}}(\alpha)\phi_r\dot{x}(\alpha)\mathrm{d}\alpha$ which reduces the results' conservative. Then, Wirtinger-based inequalities are applied in the single integrals. On the other hand, double integral is split through Lemmas 2 and 3. It is worth noting that, system stability performance under less conservative conditions can be investigated through the aforementioned method which has better performance than [28, 33].

Theorem 2: For given positive constant λ, d, τ_M, the system (14) is asymptotically stable with H_∞ prescribed attention level γ, if there exist positive definite matrices $\boldsymbol{P}_r, \boldsymbol{Q}_r, \boldsymbol{R}_r, \boldsymbol{Z}_r, \boldsymbol{S}, \boldsymbol{W}, \boldsymbol{\Phi}$ and appropriate dimensions $\boldsymbol{X}_{1r}, \boldsymbol{X}_{2r}, \boldsymbol{X}_{3r}, \boldsymbol{X}_{4r}$ such the following matrix inequalities hold for all $r = 0, \ldots, L$:

$$\begin{bmatrix}\Xi'_{1r} & * \\ \Xi'_{21r} & \Xi'_{22r}\end{bmatrix} < 0 \quad (20)$$
$$S'_r < 0, S''_r < 0, \tilde{\Sigma}_r > 0$$

where

$$\Xi'_{21r} = [\Xi'_{2r} \ \Xi'_{3r}]^{\mathrm{T}}$$
$$\Xi'_{22r} = diag(-\tau_M^{-2}\boldsymbol{Z}_r, -(\tau_M/2)^{-2}W, -\gamma^2)$$

$$\begin{aligned}\Xi'_{1r} &= e_8^{\mathrm{T}}\mathrm{E}_{1r}e_8 - (1-d)e_{10}^{\mathrm{T}}\boldsymbol{Q}_r e_{10} + e_{11}^{\mathrm{T}}\boldsymbol{R}_r e_{11} \\ &+2e_8^{\mathrm{T}}\boldsymbol{P}_r\Xi'_{4r} - \mathrm{E}_{2r}^{\prime\mathrm{T}}\tilde{\Sigma}_r\mathrm{E}'_{2r} + \mathrm{E}_{3r}^{\prime\mathrm{T}}\tilde{\phi}_r\mathrm{E}'_{3r} - e_9^{\mathrm{T}}\Phi e_9 + \lambda e_{10}^{\mathrm{T}}\Phi e_{10}\end{aligned}$$

$$\Xi'_{2r} = \boldsymbol{Z}_r A e_8 - \boldsymbol{Z}_r B K_r C e_9 - \boldsymbol{Z}_r B K_r C e_{10} + \boldsymbol{Z}_r\tilde{F}e_{12}$$
$$\Xi'_{3r} = W A e_8 - W B K_r C e_9 - W B K_r C e_{10} + W\tilde{F}e_{12}$$
$$\Xi'_{4r} = A e_8 - B K_r C e_9 - B K_r C e_{10} + \tilde{F}e_{12}$$

$$\mathrm{E}'_{2r} = \begin{bmatrix}e_8 - e_{10} \\ e_8 + e_{10} - e_{13} \\ e_{10} - e_{11} \\ e_{10} + e_{11} - e_{15}\end{bmatrix}, \quad \mathrm{E}'_{3r} = \begin{bmatrix}\tau_M e_8 \\ e_{14}\end{bmatrix}$$

$$e_j = [\underbrace{0\ldots0}_{j-8}, 1, \underbrace{0\ldots0}_{15-j}], (j = 8, \ldots, 15)$$

Proof: For a prescribed attenuation level $\gamma > 0$, considering the disturbance $\tilde{\omega}(t)$, the cost function J can be considered as

$$J = \int_0^\infty y^{\mathrm{T}}(t)y(t) - \gamma^2\tilde{\omega}^{\mathrm{T}}(t)\tilde{\omega}(t)\mathrm{d}t \quad (21)$$

For $\tilde{\omega}(t) \in l_2[0, \infty]$ and $t > 0$ condition, we have

$$\begin{aligned}J &\leq y^{\mathrm{T}}(t)y(t) - \gamma^2\tilde{\omega}^{\mathrm{T}}(t)\tilde{\omega}(t) + \dot{V}(t) - e(t)^{\mathrm{T}}\Phi e(t) \\ &+\lambda x(t-\tau(t))^{\mathrm{T}}\Phi x(t-\tau(t))\end{aligned} \quad (22)$$

Considering the stability condition for system (14), the following condition holds:

$$y^{\mathrm{T}}(t)y(t) - \gamma^2\tilde{\omega}^{\mathrm{T}}(t)\tilde{\omega}(t) + \dot{V}(t) - e(t)^{\mathrm{T}}\Phi e(t)$$
$$+\lambda x(t-\tau(t))^{\mathrm{T}}\Phi x(t-\tau(t)) < 0 \tag{23}$$

Recalling (19), we have

$$\Omega = \xi_1'^{\mathrm{T}}(t)\Xi_r'\xi_1'(t) \tag{24}$$

where

$$\Xi_r' = \Xi_{1r}' + \Xi_{4r}'^{\mathrm{T}}\left(\tau_M^2 \boldsymbol{Z}_r + \frac{\tau_M^2}{2}W\right)\Xi_{4r}' + e_8^{\mathrm{T}}C^T C e_8,$$

$$\xi_1'(t) = \begin{bmatrix} x(t) & e(t) & x(t-\tau(t)) & x(t-\tau_M) & \omega(t) \end{bmatrix}$$
$$\frac{2}{\tau(t)}\int_{t-\tau(t)}^{t} x(\alpha)\mathrm{d}\alpha \quad \int_{t-\tau_M}^{t} x(\alpha)\mathrm{d}\alpha \quad \frac{2}{\tau_M-\tau(t)}\int_{t-\tau_M}^{t-\tau(t)} x(\alpha)\mathrm{d}\alpha \Bigg]$$

By utilising Lemma 1, inequality (20) can be satisfied. □

In this theorem, the stability of the system (14) is investigated. However, the controller of system (14) cannot be obtained in this theorem. Thus, following theorem will give the method to design controller of system (14).

Theorem 3: For given positive constant $\lambda, \varepsilon, d, \tau_M$, system (14) is asymptotically stable with H_∞ prescribed attention level γ, if there exist positive definite $\boldsymbol{P}_r$, $\boldsymbol{Q}_r$, $\boldsymbol{R}_r$, $\boldsymbol{Z}_r$, $\boldsymbol{S}_r$, $\boldsymbol{W}_r$, $\boldsymbol{\Phi}$ and appropriate dimensions $\boldsymbol{X}_{1r}$, $\boldsymbol{X}_{2r}$, $\boldsymbol{X}_{3r}$, $\boldsymbol{X}_{4r}$, $\boldsymbol{T}_r$ such that the following matrix inequalities hold for all $r = 0, \ldots, L$:

$$\Xi'_{11r}\begin{bmatrix} \Xi_{1r}'' & * \\ \Xi_{21r}'' & \Xi_{22r}'' \end{bmatrix} < 0 \tag{25}$$
$$S'_r < 0, S''_r < 0, \tilde{\Sigma}_r > 0$$

where

$$\Xi_{21r}'' = [\tilde{\Xi}_r' \quad \tilde{\Xi}_r']^{\mathrm{T}}, \Xi''_{1r} = e_8\mathrm{E}_{1r}e_8^{\mathrm{T}} - (1-d)e_{10}\boldsymbol{Q}_r e_{10}$$
$$+ e_{11}^{\mathrm{T}}\boldsymbol{R}_r e_{11} + 2e_8\tilde{\Xi}_r'^T - \mathrm{E}_{2r}'^{\mathrm{T}}\tilde{\Sigma}_r\mathrm{E}_{2r}' + \mathrm{E}_{3r}'^{\mathrm{T}}\tilde{\phi}_r\mathrm{E}_{3r}' - e_9\Phi e_9^{\mathrm{T}}$$
$$+ \lambda e_{10}\Phi e_{10}^{\mathrm{T}}, \Xi_{22r}'' = \mathrm{diag}(-\tau_M^2\boldsymbol{P}_r - \boldsymbol{Z}_r, -(\tau_M/2)^{-2}\boldsymbol{P}_r - W,$$
$$-\gamma^2), \tilde{\Xi}_r' = \boldsymbol{P}_r A e_8 - \tilde{K}_r C e_9 - \tilde{K}_r C e_{10} + \boldsymbol{P}_r\tilde{F} e_{12},$$
$$\tilde{K}_r = \boldsymbol{P}_r B K_r$$

Proof: Pre-multiplying and post-multiplying both side in (20) with $\mathrm{diag}(\underbrace{I, \ldots, I}_{5}, \boldsymbol{P}_r, P, I)$, and utilising the fact that if $Z < 0$, and $Y^T = Y$ can be satisfied, the $Y^{\mathrm{T}}ZY \leq -2Y - Z^{-1}$ can be obtained, then condition (25) can be proved. Therefore, the system (14) based on event-triggered scheme and GSMC is stochastically stable with H_∞ prescribed attention level γ, and the controller gain can be designed as K_r. □

Remark 5: To keep better stability performance, the minimum H_∞ performance index γ needs to be considered. Thus, the following constrained optimisation problem holds for

$$\min \delta$$
$$\text{s.t.} \left\{ \Xi'_{11r} < 0, S'_r < 0, S''_r < 0, \tilde{\Sigma}_r > 0 \right. \tag{26}$$

where $\delta = \gamma^2$.

Next, the global sliding mode controller will be investigated by the following theorem.

Theorem 4: A decentralised switching control law can be designed to guarantee the reaching condition $s(t)\dot{s}(t) < 0$ to be satisfied

$$u(t) = -KCx(t) - (GB)^{-1}\|G\hat{F}\|(k_1\mathrm{sgn}(s(t)) + k_2 s(t))$$
$$+ k_3(GB)^{-1}\dot{f}(t) \tag{27}$$

where

$$\mathrm{sgn}(s(t)) = \begin{cases} -1, & \text{if } s(t) < 0 \\ 0, & \text{if } s(t) = 0 \\ 1, & \text{if } s(t) > 0 \end{cases}$$

Proof: Constructing the following Lyapunov function:

$$V(t) = \frac{1}{2}s^{\mathrm{T}}(t)s(t) \tag{28}$$

Then, combining (1) and (27), $\dot{V}(t) < 0$ can be further obtained. Moreover, one can conclude that reaching condition can be ensured by the designed controller.□

In Theorem 4, the global sliding mode controller is designed. It forces the state trajectories to move towards global sliding mode surface within a finite time. Moreover, it can improve the system's transient performance greatly.

Remark 6: Notice that the event-triggered scheme is characterised by parameters λ and Φ in (8). Moreover, it will affect the network usage and control performance [22, 23]. Specifically, if $\lambda = 0$, the event-triggered scheme will lose its controlling influence. Most often, it always is pre-given by researchers in power systems investigation. To adjust the trigger parameters with different conditions, an algorithm needs to be developed.

Remark 7: QGA is a global search algorithm and it has the advantages of both quantum computing and the GA. It should be noted that QGA is a highly parallelisable algorithm. Besides, it is economical and practical. Thus, QGA is introduced into this paper to optimise the event-triggered threshold. Different event-triggered threshold will generate different attenuation level of the LFC scheme. Based on the QGA, a better control strategy with a lower attenuation level will be obtained.

3.2 Quantum genetic algorithm

QGA combines quantum computing with a GA, so that it has more rapid global search capability and less counting time. By utilising quantum encoding, the quantum chromosome with multiple states is generated in QGA. Thus, it will be adopted in the following.
Quantum bit:
Quantum bit is the smallest information unit in QGA. There are two states of a quantum bit of 0 and 1, and it will be expressed as the following linear combination of basis states:

$$|Y\rangle = \alpha|0\rangle + \beta|1\rangle \tag{29}$$

where $\alpha^2 + \beta^2 = 1$, α^2 and β^2 denote the probability of the qubit amplitudes in the state of 0 and 1, respectively. If set the (α, β) initial value as $(1/\sqrt{2}, 1/\sqrt{2})$, it means that the state represented by chromosome has equal probability.
Quantum chromosome:
In QGA, the practical implementation is described as a matrix :

$$|0\rangle = \begin{pmatrix} 1 \\ 0 \end{pmatrix}, \quad |1\rangle = \begin{pmatrix} 0 \\ 1 \end{pmatrix}, \quad |Y\rangle = \begin{pmatrix} \alpha \\ \beta \end{pmatrix} \tag{30}$$

A quantum chromosome is described as a structured set containing N. The system can be described as

$$q_j^t = \begin{bmatrix} Y_{11}^t \mid & Y_{12}^t \mid & \ldots & Y_{m1}^t \mid & \ldots & Y_{mk}^t \end{bmatrix} \tag{31}$$

where q^t_j indicates the tth generation and jth chromosome. $H(t) = \{Q_1^t, Q_2^t, \ldots Q_h^t\}$, $(h = 1, 2, \ldots, l)$ where h is the size of the population $Q_l(t) = \{q_1^t, q_2^t, \ldots q_j^t, \ldots, q_n^t\}$, n is the number of

Table 1 Selection strategy of quantum gate rotation angle

| z_i | $best_i$ | f(z)< f(best) | $\Delta\theta_i$ | $s(\alpha_i, \beta_i)$ | | | |
				$\alpha_i\beta_i < 0$	$\alpha_i\beta_i > 0$	$\alpha_i = 0$	$\beta_i = 0$
0	0	FALSE	0	0	0	0	0
0	0	TRUE	0	0	0	0	0
0	1	FALSE	0.01π	+1	−1	0	±1
0	1	TRUE	0.01π	−1	+1	±1	0
1	0	FALSE	0.01π	−1	+1	±1	0
1	0	TRUE	0.01π	+1	−1	0	±1
1	1	FALSE	0.01π	0	0	0	0
1	1	TRUE	0.01π	0	0	0	0

Fig. 2 *Flowchart of QGA in optimising event-triggered scheme*

generator unit, t is the evolution generation. At the same time, a common solution set $S(t)$ is generated by observing the state of $H(t)$. For the tth generation, $S(t) = \{P_1^t, P_2^t, \ldots P_j^t, \ldots, P_n^t\}$, $P(t) = \{z_1^t, z_2^t, \ldots, z_j^t, \ldots, z_n^t\}$. $P(t)$ is the solution for every $Q(t)$.

Updating of quantum gate:

Quantum gate is the executive mechanism of evolution operation. It can be selected by different conditions. There are various quantum gates, such as not gate, controller not gate, rotation gate and so on. According to the computing characteristics of QGA, quantum rotation gate can be used appropriately. The quantum rotation gate operating can be expressed as given in Table 1

$$U(\theta_i) = \begin{bmatrix} \cos(\theta_i) & -\sin(\theta_i) \\ \sin(\theta_i) & \cos(\theta_i) \end{bmatrix} \qquad (32)$$

where z_i and $best_i$ indicate the ith code of the current chromosome and optimal chromosome, respectively, $f(z_i)$ represents fitness value, $f(best_i)$ represents the optimal fitness value, $s(\alpha_i, \beta_i)$ is the direction of rotation angle, $\Delta\theta_i$ means the values of rotation angle. If $f(z) < f(\text{best})$, adjusting q_j^t make the (α_i, β_i) evolving to the direction with outcome of z_i; otherwise, it will move to the direction of outcome of *best*.

The process of ith qubit updating as

$$\begin{bmatrix} \alpha_i' \\ \beta_i' \end{bmatrix} = U(\theta_i)\begin{bmatrix} \alpha_i \\ \beta_i \end{bmatrix} = \begin{bmatrix} \cos(\theta_i) & -\sin(\theta_i) \\ \sin(\theta_i) & \cos(\theta_i) \end{bmatrix}\begin{bmatrix} \alpha_i \\ \beta_i \end{bmatrix} \qquad (33)$$

where θ_i is the quantum gate rotation angle, it is taken as the following control strategy.

The steps of QGA

Step 1: Initialing population $Q(t_0)$, and randomly generate chromosome with the number of n;
Step 2: Measuring every individual in $Q(t_0)$, and obtain the determine solution $P(t_0)$ for every $Q(t_0)$;
Step 3: Achieving fitness evaluation for every $P(t_0)$;
Step 4: Recording the best individual and corresponding fitness evaluation; if the number of itreation is n, stop, else continue the following step;
Step 5: Measuring each individual in $Q(t)$ and getting the determine solution;
Step 6: Assessing the new fitness;
Step 7: Applying the quantum gate to update the individual q_j^t in $Q(t)$ and obtain the new population $Q(t + 1)$; and return Step 4.

This algorithm flow which QGA applied into the proposed method to optimise event-triggered threshold is shown in Fig. 2.

Remark 8: It should be noted that logic gate of the probability amplitude was applied to maintain the diversity of population in QGA. It is better than the mating, mutation and other proposed gate in the traditional GA [34]. By utilising quantum gate in QGA, the starting state can be transformed into ending state. Moreover, QGA is a state transform process in which the optimising of objection can be achieved.

4 Case study and discussion

In this section, two simulation examples are carried out to verify the effectiveness of the proposed method. In the first case, the load disturbances are applied to LFC for two-area power system with the proposed method under network conditions. In this case, the stability and robust performance of the proposed control method for multi-area power system are demonstrated. To illustrate the efficiency of the proposed control scheme with a more realistic power system model, Kundur's two-area test system which has four synchronous generators is implemented in second case. In the second case, this test system is divided into two control areas to convert it into a multi-area power system. Further, it is assumed that only one generator in each area is responsible for the LFC task, i.e. $G1$ in area 1, $G3$ in area 2.

4.1 Case 1

To demonstrate the usage and effectiveness of the proposed method, a two-area power system is considered in this case, as shown in Fig. 3. At the same time, the parameters of this model are listed in Table 2.

In this case, the transition probability matrix is set as follows:

$$P = \begin{bmatrix} 0.5088 & 0.4912 \\ 0.4286 & 0.5714 \end{bmatrix}$$

and it is plotted in Fig. 4.

Seting $G_1 = G_2 = [-1 \quad 1 \quad -1 \quad 1 \quad 1 \quad 1 \quad 1]$, $f(t) = -0.1653e^{-1000t}$, and $T_{12} = 0.1986$. By solving Theorem 1, the results of delay stability margin are shown in Table 3. For different controller gains, different results are proposed in kinds of literature. For brevity, by the comparisons with [35, 36], the delay stability margins are given for two-area LFC power system in Table 3. It can be observed from Table 3 that the maximum delay upper bounds of transmission time delay obtained by this proposed method is larger than those computed in [35, 36] with different
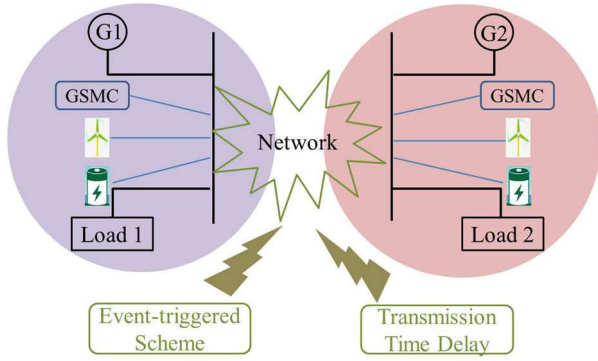
Fig. 3 *Block diagram of two-area power system*

Table 2 Parameters of the two-area LFC scheme

Area	R	M	D	T_g	T_{ch}	T_{wi}	T_{ESi}
1	0.05	10.0	1.0	0.1	0.3	1.5	0.0352
2	0.05	12.0	1.5	0.17	0.4	1.8	0.0352
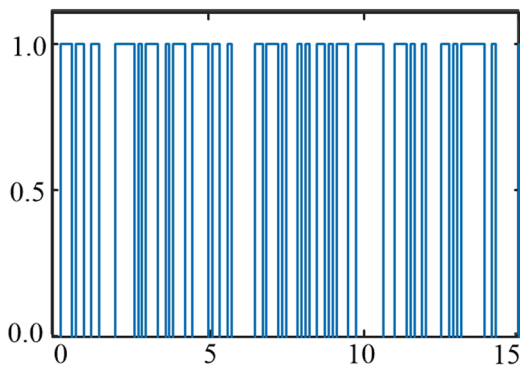
Fig. 4 *Random transmission delays*

Table 3 Transmission time delay upper bound comparison

K_I	K_p	$d = 0.0$			$d = 0.5$		
		Theorem 1	[35]	[36]	Theorem 1	[35]	[36]
0.0	0.1	15.99	13.77	13.77	14.01	11.72	12.88
0.0	0.2	9.06	6.69	6.69	7.94	5.55	6.14
0.0	0.4	2.72	3.12	3.12	2.44	2.36	2.68
0.1	0.1	17.66	13.68	13.69	12.73	11.63	12.58
0.1	0.2	9.7	6.94	6.94	7.72	5.83	6.34
0.1	0.4	3.32	3.29	3.29	2.85	2.55	2.83

disturbance conditions, for power system with constant delay ($d = 0.0$) and time-varying delays ($d = 0.5$). That is to say, the presented results are less conservative than those in existing literature [35, 36]. Therefore, the proposed method – improved Lyapunov function and Wirtinger inequality – has better performance in calculating the maximum delay upper bound under stable condition.

By utilising QGA with $\theta = (\pi/4)$ and the generation, population and length of genes set as 200, 40 and 20, respectively. When $\lambda = 0.23813$, the optimised disturbance attenuation level $\gamma = 3.18249$ can be obtained, by combining Remark 5 with QGA. This optimise algorithm procedure is plotted in Fig. 5a. In light of Remark 5 with $\lambda = 0.23813$, the different area global sliding mode controller gain can be figured out as follows:

Area 1:

$$K_{11}(t) = [0.2743, 0.0706], K_{12}(t) = [0.2726, 0.0730]$$

Area 2:

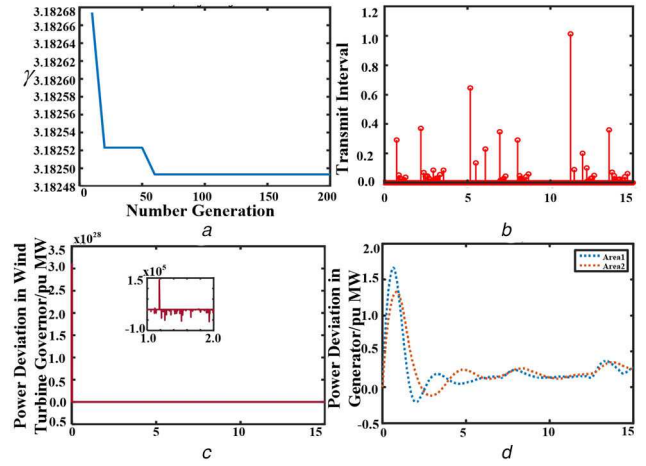$$K_{21}(t) = [0.3026, 0.4624], K_{22}(t) = [0.3009, 0.4745]$$

Fig. 5 *The performance of designed model in Case 1*
(a) Optimisation algorithm performance, *(b)* Release instant and release intervals for Area 2, *(c)* Wind turbine governor output power deviation, *(d)* Generator output power deviation for Area 1 and Area 2
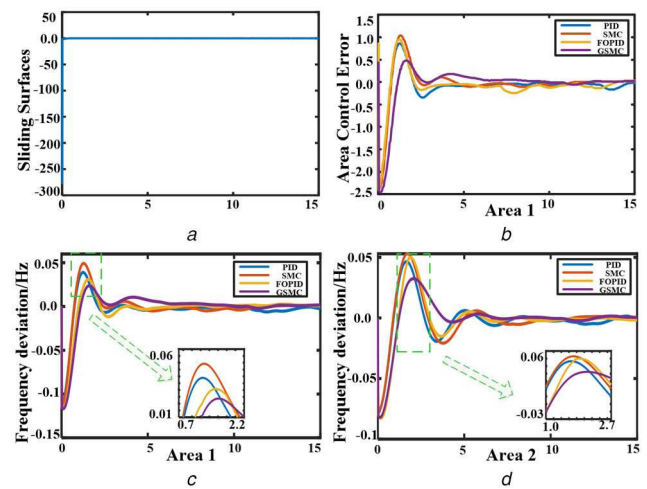

Fig. 6 *Results of Case 1*
(a) Sliding surfaces, *(b)* ACE of Area 1, *(c)* Frequency deviations of Area 1 with step load disturbances, *(d)* Frequency deviations of Area 2 with step load disturbances

By utilising Matlab/Simulink Toolbox, the simulation platform is built. The wind turbine induction generator is utilised in this simulation platform, and the wind speed and trip coefficient set as 9 m/s and 0.2, respectively. For simulation purposes a non-periodic phase signal disturbance is implemented at $t = 0$ with $\Delta P_d = 0.1 \, \text{p.u.} \, \text{MW}$. To scrutinise the effectiveness of the proposed event-triggered scheme designed by QGA, release time instants, and intervals are shown in Fig. 5b. It can be concluded that the proposed resilient event-triggered scheme can reduce the number of control updates. Therefore, this method can reduce the utilisation of network, and increase the network's bandwidth. To validate the effectiveness of the proposed event-triggered GSMC scheme, the proposed method is compared with event-triggered fractional order PID control (FOPID) [8], event-triggered SMC [12] and event-triggered PID control. Figs. 5c and d depict the power deviation of wind turbine governor and generators, respectively. Fig. 6a describes the sliding surfaces which converges to zero in a short time. It demonstrates that the sliding control system reaches the sliding surfaces asymptotically and remains on sliding surfaces. Figs. 6b–d illustrate the comparison results in ACE and the frequency deviations of the proposed global sliding mode controller versus the existing FOPID, SMC and PID under the event-triggered scheme. It can be seen that the event-triggered GSMC scheme exhibits better performance of lower amplitude and faster damping of the frequency deviations than recently developed techniques. In this case, the event-triggered global sliding mode controller is designed as the following:

Area 1:

$$u(t) = -K_{1i}Cx(t) - (GB)^{-1} \| \hat{GF} \| (3.0\text{sgn}(s(t)) + 3.0s(t)) + 3.0(GB)^{-1}\dot{f}(t)$$

Area 2:

$$u(t) = -K_{2i}Cx(t) - (GB)^{-1} \| \hat{GF} \| (2.5\text{sgn}(s(t)) + 3.0s(t)) + 2.5(GB)^{-1}\dot{f}(t)$$

The event-triggered sliding mode controller is the same as event-triggered global sliding mode controller, except that there is no $f(t)$.

The event-triggered FOPID controller can be designed as

$$u(s) = K_p + K_I\frac{1}{s^\iota} + K_D s^\nu$$

Area 1:

$$K_{11}(K_p, K_I, K_D, \iota, \tau) = [0.2743, 0.0706, 0.05, 1.2, 0.7],$$
$$K_{12}(K_p, K_I, K_D, \iota, \tau) = [0.2726, 0.0730, 0.05, 1.2, 0.7]$$

Area 2:

$$K_{21}(K_p, K_I, K_D, \iota, \tau) = [0.3026, 0.4624, 0.05, 1.2, 0.7],$$
$$K_{22}(K_p, K_I, K_D, \iota, \tau) = [0.3009, 0.4745, 0.05, 1.2, 0.7]$$

The event-triggered PID controller can be designed as

$$u(s) = K_p + K_I\frac{1}{s} + K_D s$$

Area 1:

$$K_{11}(K_p, K_I, K_D) = [0.2743, 0.0706, 0.05],$$
$$K_{12}(K_p, K_I, K_D) = [0.2726, 0.0730, 0.05]$$

Area 2:

$$K_{21}(K_p, K_I, K_D) = [0.3026, 0.4624, 0.05],$$
$$K_{22}(K_p, K_I, K_D) = [0.3009, 0.4745, 0.05]$$

It should be noted that parameter uncertainty is a major issue for power systems, and the robustness plays an essential part in control techniques. In this way, to demonstrate the efficacy of the proposed event-triggered GSMC further, the robustness of controller with case of $\pm 50\%$ parameter uncertainty will be considered. Figs. 7a and b illustrate the frequency deviation response for $+50\%$ upper bound in all parameters of Areas 1 and 2. Comparison frequency deviation response for -50% lower bound in all parameters of Areas 1 and 2 are shown in Figs. 7c and d. It can be inferred that the proposed event-triggered GSMC is highly robust as compared to above existing control schemes. Consequently, it can be claimed that the proposed approach provides excellent robustness.

4.2 Case 2

To introduce the effectiveness of the proposed control scheme with a more realistic power system model, Kundur's two-area system which has 4 synchronous generators and 11 buses is considered as shown in Fig. 8. It is assumed that only one generator in each area is responsible for the LFC task, i.e. $G1$ in area 1, $G3$ in area 2. To investigate the effectiveness of the proposed event-triggered GSMC, frequency deviation is compared with that of existing event-triggered SMC technique, the step load disturbances are taken as 0.38 p.u. MW on bus 8 at $t = 5$ s. In this case, the designed event-triggered global sliding mode controller and event-triggered sliding mode controller have same controller gain as Case 1. Proposed Kundur's two-area system has the same parameters as given in [37].
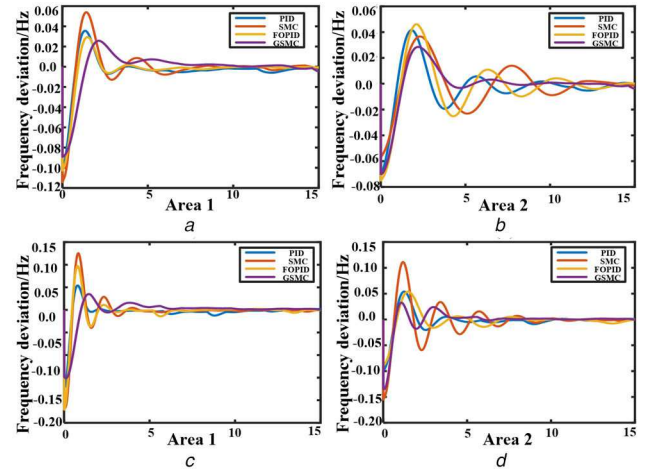

Fig. 7 *Results of Case 1 with ±50% parameter uncertainty*
(a) Frequency deviations of Area 1 with +50% uncertainty parameter, *(b)* Frequency deviations of Area 2 with +50% uncertainty parameter, *(c)* Frequency deviations of Area 1 with −50% uncertainty parameter, *(d)* Frequency deviations of Area 2 with −50% uncertainty parameter
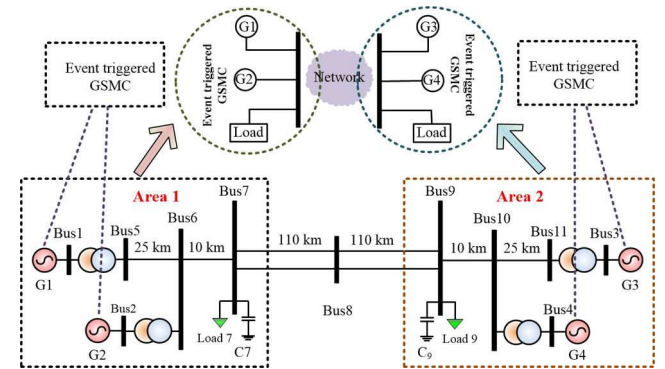

Fig. 8 *Event-triggered GSMC for two-area four-machine power system*

Figs. 9a and b illustrate the frequency and tie-line power derivation for the two control areas of event-triggered GSMC and event-triggered SMC. It can be inferred that the frequency deviations can be settled to zero quickly with a much better transient performance in the power system utilising the proposed method. Hence, it can be concluded that the proposed GSMC with event-triggered scheme exhibits a better performance over the existing control technique. Meantime, the relative rotor angles of generator $G2$ to generator $G1$ are decreased, and relative rotor angles of $G3$ and $G4$ to generator $G1$ are increased, especially these results can restore at around $t = 10$ s under the proposed method, as given in Fig. 9c. As can be seen from Fig. 9d, the frequency of four generators has large overshoot, then the system with proposed event-triggered GSMC scheme can restore the four generator's frequency to around at 60.36 Hz. Therefore, this test demonstrates the effectiveness of the proposed event-triggered GSMC in stabilising the power system.

5 Conclusion

An efficient LFC scheme is a great need for the electric power system to counter the ever-increasing complexity of power systems. In this paper, the LFC scheme with transmission time delays and external disturbances has been modelled as Markov jump linear system. Based on this model, the criteria of stability and stabilisation for this system have been derived by improved Lyapunov function and Wirtinger-based inequality. It can be demonstrated that the upper bound of time delay obtained in this paper is larger than other results computed in existing literature. Thus, the results obtained in this paper are less conservative than those in other papers. Moreover, the LFC scheme considering event-triggered scheme and GSMC has been investigated in this paper. Different from the existing event-triggered scheme, the
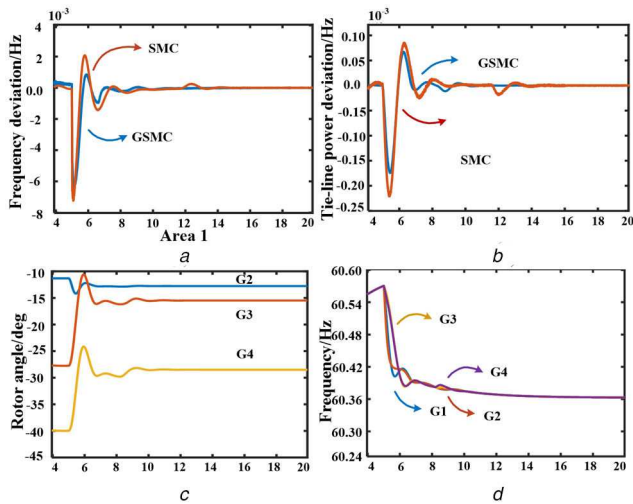
Fig. 9 *Results of Case 2*
(a) Frequency deviations, *(b)* Tie-line power derivations, *(c)* Relative angles of *G*2, *G*3 and *G*4 to *G*1, *(d)* Frequency

QGA has been applied to this paper making it can be adjusted by different conditions. It is demonstrated that the proposed event-triggered global sliding mode controller shows better robustness towards $\pm 50\%$ parameter uncertainty and external disturbances rejection capability than the existing techniques. Besides, the effectiveness of the proposed event-triggered GSMC has verified in Kundur's two-area power system.

6 Acknowledgments

7 References

[1] Ramachandran, R., Madasamy, B., Veerasamy, V.*, et al.*: 'Load frequency control of a dynamic interconnected power system using generalized Hopfield neural network-based self-adaptive PID controller', *IET Gener. Transm. Distrib.*, 2018, **12**, (21), pp. 5713–5722

[2] Yu, D., Zhu, H., Han, W.*, et al.*: 'Dynamic multi agent-based management and load frequency control of PV/fuel cell/wind turbine/CHP in autonomous microgrid system', *Energy*, 2019, **173**, (15), pp. 554–568

[3] Lv, X., Sun, Y., Wang, Y.*, et al.*: 'Adaptive event-triggered load frequency control of multi-area power systems under networked environment via sliding mode control', *IEEE Access*, 2020, **8**, (1), pp. 86585–86594

[4] Guha, D., Roy, K.P., Banerjee, S.: 'Maiden application of SSA-optimised CC-TID controller for load frequency control of power systems', *IET Gener. Transm. Distrib.*, 2019, **13**, (7), pp. 1110–1120

[5] Mi, Y., Hao, X., Liu, Y.*, et al.*: 'Sliding mode load frequency control for multi-area time-delay power system with wind power integration', *IET Gener. Transm. Distrib.*, 2017, **11**, (18), pp. 4644–4653

[6] Choi, J.W., Heo, S.Y., Kim, K.M.: 'Hybrid operation strategy of wind energy storage system for power grid frequency regulation', *IET Gener. Transm. Distrib.*, 2016, **10**, (3), pp. 736–749

[7] Tan, W., Fu, C.: 'Linear active disturbance-rejection control: analysis and tuning via IMC', *IEEE Trans. Ind. Electron.*, 2016, **63**, (4), pp. 2350–2359

[8] Sondhi, S., Hote, V.Y.: 'Fractional order PID controller for load frequency control', *Energy Convers. Manag.*, 2014, **85**, pp. 343–353

[9] Yang, J., Sun, X., Liao, K.*, et al.*: 'Model predictive control-based load frequency control for power systems with wind-turbine generators', *IET Renew. Power Gener.*, 2019, **13**, (15), pp. 2871–2879

[10] Onyeka, E.A., Yan, X., Mao, Z.*, et al.*: 'Robust decentralized load frequency control for interconnected time delay power systems using sliding mode techniques', *IET Control. Theory Appl.*, 2020, **14**, (3), pp. 470–480

[11] Li, H., Wang, X., Xiao, J.: 'Adaptive event-triggered load frequency control for interconnected microgrids by observer-based sliding mode control', *IEEE Access*, 2019, **7**, pp. 68271–68280

[12] Sun, Y., Wang, Y., Wei, Z.*, et al.*: 'Robust H_∞ load frequency control of multi-area power system with time delay: a sliding mode control approach', *IEEE J. Autom. Sin.*, 2018, **5**, (2), pp. 610–617

[13] Ramadan, H., Fathy, A., Becherif, M.: 'Optimal gain scheduling of VSC-HVDC system sliding mode control via artificial bee colony and mine blast algorithms', *IET Gener. Transm. Distrib.*, 2018, **12**, (3), pp. 661–669

[14] Mohanty, A., Patra, S., Ray, P.: 'Robust fuzzy-sliding mode based UPFC controller for transient stability analysis in autonomous wind-diesel-PV hybrid system', *IET Gener. Transm. Distrib.*, 2016, **10**, (5), pp. 1248–1257

[15] Mu, C., Tang, Y., He, H.: 'Improved sliding mode design for load frequency control of power system integrated an adaptive learning strategy', *IEEE Trans. Ind. Electron.*, 2017, **64**, (8), pp. 6742–6751

[16] Trip, S., Cucuzzella, M., Persis, C.D.*, et al.*: 'Passivity-based design of sliding modes for optimal load frequency control', *IEEE Trans. Control Syst. Technol.*, 2019, **27**, (5), pp. 1893–1906

[17] Liao, K., Xu, Y.: 'A robust load frequency control scheme for power systems based on second-order sliding mode and extended disturbance observer', *IEEE Trans. Ind. Inform.*, 2018, **14**, (7), pp. 3076–3086

[18] Fei, J., Chu, Y., Hou, S.: 'A back stepping neural global sliding mode control using fuzzy approximator for three-phase active power filter', *IEEE Access*, 2017, **5**, pp. 16021–16032

[19] Efimov, D., Fridman, L.: 'Global sliding-mode observer with adjusted gains for locally Lipschitz systems', *Automatica*, 2011, **47**, (3), pp. 565–570

[20] Wu, Z., Mo, H., Xiong, J.*, et al.*: 'Adaptive event-triggered observer-based output feedback L_∞ load frequency control for networked power system', *IEEE Trans. Ind. Inform.*, 2019, **34**, (2), pp. 1653–1656

[21] Dong, L., Tang, Y., He, H.*, et al.*: 'An event-triggered approach for load frequency control with supplementary ADP', *IEEE Trans. Power Syst.*, 2017, **32**, (1), pp. 581–589

[22] Liu, J., Gu, Y., Zha, L.*, et al.*: 'Event-triggered H_∞ load frequency control for multiarea power systems under hybrid cyber attacks', *IEEE Trans. Syst. Man. Cy - S*, 2019, **49**, (8), pp. 1665–1678

[23] Wu, Z., Xu, Y., Pan, Y.*, et al.*: 'Event-triggered control for consensus problem in multi-agent systems with quantized relative state measurements and external disturbance', *IEEE Trans. Circuits Syst. I, Reg. Papers*, 2018, **65**, (7), pp. 2232–2242

[24] Lee, J., Lin, W., Liao, G.*, et al.*: 'Quantum genetic algorithm for dynamic economic dispatch with valve-point effects and including wind power system', *Int. J. Electr. Power Energy Syst.*, 2011, **33**, pp. 189–197

[25] Laboudi, Z., Chikhi, S.: 'Comparison of genetic algorithm and quantum genetic algorithm', *Int. Arab J. Inf. Techn.*, 2012, **9**, (3), pp. 243–249

[26] Ning, T., Jin, H., Song, X.*, et al.*: 'An improved quantum genetic algorithm based on MAGTD for dynamic FJSP', *J. Amb. Intel. Hum. Comp.*, 2018, **9**, (4), pp. 931–940

[27] Deng, L., Zhu, H., Zhou, Q.*, et al.*: 'Adaptive top-hat filter based on quantum genetic algorithm for infrared small target detection', *Multimed. Tools Appl.*, 2018, **77**, (9), pp. 10539–10551

[28] Wen, S., Yu, X., Zeng, Z.*, et al.*: 'Event-triggering load frequency for multiarea power systems with communication delays', *IEEE Trans. Ind. Electron.*, 2016, **63**, (2), pp. 1308–1317

[29] Sun, Y., Zhai, S., Cui, T.*, et al.*: 'Frequency regulation strategy for private EVs participating in integrated power system of REs considering adaptive Markov transition probability', *Electr. Pow. Syst. Res.*, 2019, **17**, (3), pp. 291–301

[30] Li, Z., Zang, C., Zeng, P.*, et al.*: 'Control of a grid-forming inverter based on sliding-mode and mixed H_2/H_∞ control', *IEEE Trans. Ind. Electron.*, 2017, **64**, (5), pp. 3862–3872

[31] Sun, Y., Li, N., Zhao, X.*, et al.*: 'Robust H_∞ load frequency control of delayed multi-area power system with stochastic disturbances', *Neurocomputing*, 2016, **193**, pp. 58–67

[32] Seuret, A., Gouaisbaut, F.: 'Wirtinger-based integral inequality: application to time-delay systems', *Automatica*, 2013, **49**, (9), pp. 2860–2866

[33] Vafamand, N., Khooban, M.H., Dragicevic, T.*, et al.*: 'Time-delayed stabilizing secondary load frequency control of shipboard microgrid', *IEEE Syst. J.*, 2019, **13**, (3), pp. 3233–3241

[34] Friedrich, T., Kotzing, T., Krejca, M.S.*, et al.*: 'The compact genetic algorithm is efficient under extreme gaussian noise', *IEEE Trans. Evol. Comput.*, 2017, **21**, (3), pp. 477–490

[35] Jiang, L., Yao, W., Wu, H.Q.*, et al.*: 'Delay-dependent stability for load frequency control with constant and time-varying delays', *IEEE Trans. Power Syst.*, 2012, **27**, (2), pp. 932–941

[36] Ramakrishnan, K., Ray, G.: 'Stability criteria for nonlinearly perturbed load frequency systems with time-delay', *IEEE J. Emerg. Sel. Topics Circuits Syst.*, 2015, **5**, (3), pp. 383–392

[37] Cao, S., Lin, N., Dinavahi, V.: 'Faster-than-real-time dynamic simulation of AC/DC grids on reconfigurable hardware', *IEEE Trans. Power Syst.*, 2019, **35**, (2), pp. 1539–1548